Atmospheric Environment 97 (2014) 182–194

Contents lists available at ScienceDirect

Atmospheric Environment

journal homepage: www.elsevier.com/locate/atmosenv

Source contributions to primary and secondary inorganic particulate matter during a severe wintertime $PM_{2.5}$ pollution episode in Xi'an, China

Dexiang Wang [a], Jianlin Hu [b], Yong Xu [a], Di Lv [a], Xiaoyang Xie [a], Michael Kleeman [b], Jia Xing [c], Hongliang Zhang [b, d, *], Qi Ying [e, **]

[a] College of Forestry, Northwest A&F University, Yangling, Shaanxi 712100, China
[b] Department of Civil and Environmental Engineering, University of California, Davis, CA 95616, USA
[c] Atmospheric Modeling and Analysis Division, National Exposure Research Laboratory, US Environmental Protection Agency, Research Triangle Park, NC 27711, USA
[d] Department of Civil and Environmental Engineering, Louisiana State University, Baton Rouge, LA 70803, USA
[e] Zachry Department of Civil Engineering, Texas A&M University, College Station, TX 77843, USA

HIGHLIGHTS

- An extremely high $PM_{2.5}$ concentrations episode in January 2013 was simulated.
- Source contributions to primary/secondary inorganic PM in Xi'an were quantified.
- Industrial and residential activities are the dominating sources for primary species.
- Energy production industries are the major source for secondary nitrate/sulfate.

ARTICLE INFO

Article history:
Received 31 May 2014
Received in revised form
8 August 2014
Accepted 11 August 2014
Available online 11 August 2014

Keywords:
Xi'an
Source apportionment
Particulate matter
WRF/CMAQ
EDGAR

ABSTRACT

Average $PM_{2.5}$ concentrations of ~250 μg m^{-3} and peak concentrations of ~500 μg m^{-3} were observed in Xi'an, the largest city in Northwest China during an extreme event in January 2013. The source-oriented versions of the Community Multi-scale Air Quality (CMAQ) model with anthropogenic emissions from Emissions Database for Global Atmospheric Research (EDGAR) were used to study the source contributions of six different source categories including energy production, industries, transportation, residential activities, "other" (agriculture, biomass, waste burning, and biogenic sources), and windblown dust to primary and secondary inorganic $PM_{2.5}$ (nitrate and sulfate) during this episode. The model generally captured the variation and magnitude of $PM_{2.5}$ concentrations at monitoring sites. The monthly average concentration of the predicted $PM_{2.5}$ in Xi'an was >200 μg m^{-3}, comparing favorably with the measurement of ~250 μg m^{-3}. Predicted concentrations of elemental carbon (EC), organic aerosol (OA), sulfate, nitrate, and ammonium were 6, 35, 18, 22, and 12 μg m^{-3}, respectively. Chemically unresolved $PM_{2.5}$ components ($PM_{2.5}$ Other) were ~80 μg m^{-3}. Industries and residential activities dominated EC, organic carbon (OC) and $PM_{2.5}$ Other, contributing 85%, 95%, and 83%, respectively. Energy production (mainly coal combustion) was the dominating source for secondary nitrate, contributing 46%. Other local and upwind sources were also important, contributing 43% and 11% of total nitrate, respectively. Primary sulfate was ~10 μg m^{-3} in vicinity surrounding point sources. Secondary sulfate from upwind sources was also important with concentrations of ~4–5 μg m^{-3}. Secondary sulfate formed by SO_2 emitted from local sources was dominated by energy production. Based on the contributions of different sources to primary components and secondary nitrate and sulfate, the contributions of different sources to $PM_{2.5}$ total mass in Xi'an during the extremely polluted months are: energy 5%, industries 58%, transportation

* Corresponding author. Department of Civil and Environmental Engineering, Louisiana State University, Baton Rouge, LA 70803, USA.
** Corresponding author.
E-mail addresses: tamzhang@ucdavis.edu, hlzhang@lsu.edu (H. Zhang), qying@civil.tamu.edu (Q. Ying).

http://dx.doi.org/10.1016/j.atmosenv.2014.08.020

2%, residential activities 16%, dust 4%, and other (including other components, inexplicit sources, and upwind sources) 15%.

1. Introduction

Extremely high levels of airborne particulate matter (PM) in China have been reported as a result of the rapid economic growth and urbanization without sufficient controls on pollutant emissions. Sustained exposure to air pollution causes respiratory diseases and significantly reduces life expectancy (Chen et al., 2013; Poschl, 2005). To protect the public health, the Chinese Central Government and Ministry of Environmental Protection (MEP) has taken urgent actions to set up new air quality standards by adopting $PM_{2.5}$ as a new criteria pollutant and formulating the Atmospheric Pollution Prevention Action Plan (MEP, 2012a,b). Since early 2013, real time measurements of criteria pollutants including $PM_{2.5}$ and PM_{10} in all the large cities have been made available to the public (Hu et al., 2014; Wang et al., 2014). Understanding the formation processes and source contributions of $PM_{2.5}$ pollution in regions with significantly different economies, terrain and climate is crucial for developing effective emissions reduction plans. While many studies have been conducted on this topic, the majority have either focused on the entire East Asia region with relative low spatial resolution (Tang et al., 2004; Wang et al., 2010; Yamaji et al., 2006; Zhang et al., 2012) or the most economically developed areas of China such as Beijing and surrounding areas (An et al., 2007; Chen et al., 2007; Streets et al., 2007; Xing et al., 2011), the Yangtze River Delta area (Li et al., 2008, 2011; Tie et al., 2009), and the Pearl River Delta (Fan et al., 2011; Feng et al., 2007; Wang et al., 2013b; Wei et al., 2012; Wu et al., 2012). Few studies have been conducted for other parts of China, such as the Central and Western regions.

Xi'an is the Provincial capital of Shaanxi Province and the largest city in Northwest China with a population of more than 8 million. It is located in the center of the Guanzhong Plain with a topographic basin surrounded by the Qinling Mountains to the south and the Loess Plateau to the north. High emissions from anthropogenic sources such as coal combustion, transportation and industries combined with limited ventilation capability in the air basin can lead to elevated concentrations of pollutants in the atmosphere, especially during stagnation events. Windblown dust from the Loess Plateau can significantly aggravate the pollution during periods with higher wind speeds (Wang et al., 2012).

Only a few studies have been carried out to characterize the atmospheric aerosols in Xi'an and the Guanzhong plain area. Secondary inorganic aerosol including sulfate, nitrate, and ammonium were shown to account for a significant portion (20–60%) of the total PM (Zhang et al., 2002). Local coal combustion and vehicle emissions were identified to be the main sources of carbonaceous particles (Cao et al., 2009, 2005; Han et al., 2009). However, quantitative contributions of emissions sources to the primary and the secondary PM components over a regional scale are not available to assist policy makers to formulate efficient control strategies.

An extremely severe air pollution event swept across the Northern China in January 2013, exposing 0.6 billion people to unhealthy levels of pollution. In Xi'an, maximum hourly $PM_{2.5}$ concentrations higher than 700 $\mu g\ m^{-3}$ were observed, with monthly average concentrations measured to be ~250 $\mu g\ m^{-3}$. Quan et al. (2014) found that PBL height in haze days of this month was lower compared to normal days, leading to an increase in the surface aerosol concentrations and higher heterogeneous conversions of NO_x and SO_2 from gas to particle phases were observed. Wang et al. (2013a) simulated the month over Beijing–Tianjing–Hebei area and pointed out industrial and domestic sources are the major local sources and regional contributions of domestic and agricultural sources from provinces to the south are also important. Although these two studies provide insights to the formation and sources contributing to the main pollutants during this event, there is lack of understanding of the sources that are responsible for the observed high $PM_{2.5}$ concentrations over the Xi'an region.

Source-oriented chemical transport models (CTMs) are able to quantitatively predict regional source contributions to primary and secondary PM mass and component concentrations by directly tracking the emission, transport, chemical transformation and removal processes of primary PM and secondary PM precursors from different emission categories or regions (Berglen et al., 2004; Kleeman and Cass, 2001; Napelenok et al., 2006; Ying and Kleeman, 2006; Zhang et al., 2014b). The Community Multi-scale Air Quality (CMAQ) model maintained by US EPA is widely used by researchers around the world due to its open-source framework that easily allows for inclusion of user-developed features. Source-oriented versions of the CMAQ model have been developed and applied to track sources of gas phase species (Zhang et al., 2013; Zhang and Ying, 2011a), secondary inorganic PM (Zhang et al., 2012), and secondary organic aerosols (SOA) (Zhang and Ying, 2011b) in the United States and East Asia.

Here we apply the source-oriented CMAQ models based on CMAQ v4.7.1 developed in previous studies to determine the source contributions to primary and secondary PM in Xi'an during the January 2013 high $PM_{2.5}$ episode. Anthropogenic emissions extracted from a high resolution ($0.1^\circ \times 0.1^\circ$) global emission inventory are used as the starting point for the calculation. The concentrations of PM and gas species predicted by simulations of atmospheric transport, chemical reaction, phase change, and deposition are evaluated against measurements at all available surface sites in and around Xi'an. The main sources of primary PM and secondary inorganic PM components over the Xi'an region are identified. To the best of the authors' knowledge, this is the first study of regional $PM_{2.5}$ source apportionment conducted over Northwest China. Results from this paper demonstrate the ability of a state-of-the-science source-oriented CTM to act as a useful tool to investigate severe pollution events and provide crucial information needed to design effective control strategies.

2. Model description

2.1. Source-oriented CMAQ model

Three sets of simulations were conducted in the present study. The first base case simulation used the unmodified CMAQ model (v4.7.1) (Byun and Schere, 2006). The second simulation used a source-oriented CMAQ model for primary PM source apportionment and the third simulation used another modified version of source-oriented CMAQ for secondary inorganic PM source apportionment. Both source apportionment models are based on the original CMAQ v4.7.1 and use the same model options for horizontal and vertical transport, emission, and dry/wet deposition.

The source-oriented version of CMAQ for primary PM was designed to efficiently determine the contributions of many

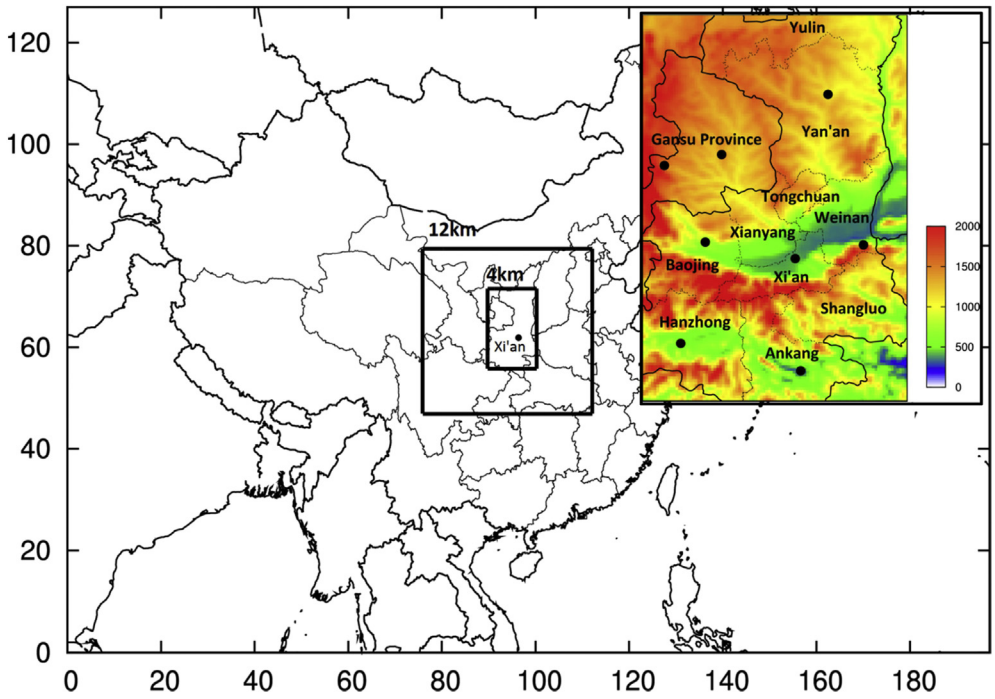

Fig. 1. Configuration of the nested CMAQ domains. The outer domain is the 36-km domain covering East Asia. Xi'an is marked as the black dot in 4-km domain. The axes indicate number of grid cells in 36-km domain. Inset shows the average terrain height (meters above mean sea level) within 4-km domain. Solid lines indicate the provincial boundaries and dashed lines indicate the city boundaries within Shaanxi Province. Black dots show the locations of meteorological sites.

sources over long periods of time by only simulating the processes of emission, transport and deposition of primary PM mass from each source in the Aitken and accumulation modes without considering the gas and particle phase chemistry and gas-to-particle formation of secondary PM. Source specific emission speciation profiles are used during the post-process step to calculate relative contributions of each chemical component to the total primary PM mass. Similar techniques have been used in previous studies for source apportionment of primary PM using the UCD/CIT model for California and Texas in the United States (Hu et al., 2013; Ying et al., 2008; Zhang and Ying, 2010). In this study, the absolute contributions of each source to total primary PM are calculated using the fractional contributions determined from the primary PM only simulations and total primary PM concentrations determined from a full chemistry simulation. This approach compensates for the changes in primary PM deposition velocity that occur when secondary PM components coat the primary particle cores.

The source-oriented version of CMAQ for secondary inorganic PM source apportionment in this study has been reported in a previous publication (Zhang et al., 2012). In general, the SAPRC99 gas phase mechanism (Carter, 2000) was expanded with additional reactions and species to separately track sulfate and nitrate precursors from different sources. The aerosol modules were modified to add source specific nitrate and sulfate species and track the formation of nitrate and sulfate from different sources separately through the gas-to-particle partitioning. It should be noted that only formation of secondary sulfate and nitrate through the oxidation of SO_2 and NO_x is tracked by the source apportionment technique.

2.2. Model configuration

Simulations are conducted from January 2, 2013 to January 30, 2013 using three-level nested domains. The first three days are used as spin-up and therefore excluded during post-processing. As shown in Fig. 1, the 36-km horizontal resolution domain (197 × 113 grid cells) covers most of China and the surrounding countries. The 12-km domain covers Shaanxi Province and surrounding areas (104 × 97 grid cells) and the 4-km domain covers most of Shaanxi Province with the capital city of Xi'an located in the middle of the domain. The same vertical resolution with 16 layers up to 20 km above ground is used for all three domains. The inset (a) of Fig. 1 shows the surface elevation of the 4-km domain with Xi'an located in an air basin that is unfavorable for pollutant dispersion.

2.3. Model inputs

The Weather Research and Forecasting (WRF) model v3.2.1 was used to generate meteorological inputs for air quality modeling. The WRF model used the same horizontal domain as the CMAQ model but specified a total of 29 vertical layers, which includes more layers in the free troposphere. The WRF Processing System (WPS) generated the initial and boundary conditions for the WRF simulations based on data from the 1° × 1° resolution NCEP FNL Operational Model Global Tropospheric Analyses dataset (available at http://rda.ucar.edu/dsszone/ds083.2/). WRF runs were conducted for seven day periods with the first day used as spin-up to reduce the influence of initial conditions from NCEP data. The physics options used to conduct the WRF runs were identical to those used in a previous WRF/CMAQ simulation for China (Zhang et al., 2014a). The Meteorology Chemistry Interface Processor (MCIP) v3.6 was used to convert WRF outputs to CMAQ ready meteorological files.

Annual anthropogenic emissions of CO, NO_x, SO_2, non-methane volatile organic compounds (NMVOC), and PM_{10} with a spatial resolution of 0.1° × 0.1° were downloaded from Emissions Database for Global Atmospheric Research (EDGAR) version 4.2 (available at http://edgar.jrc.ec.europa.eu/overview.php?v=42). The gridded EDGAR 4.2 inventories contain emissions from a number of sectors based on IPCC designations. The EDGAR v4.2 inventory does not

include $PM_{2.5}$ emissions yet. $PM_{2.5}/PM_{10}$ ratios for each source category were estimated based on Zhang et al. (2007a) and then applied to estimated $PM_{2.5}$ emissions. NMVOC and $PM_{2.5}$ emissions were mapped to model species needed by the SAPRC99 photochemical mechanism and the AERO5 aerosol module. Representative profiles for each EDGAR source category were taken from the SPECIATE 4.3, a speciation profile data base developed by the US EPA. Tables S1 and S2 show the profiles for NMVOC and $PM_{2.5}$, respectively, and the corresponding profile numbers in the SPECIATE v4.3 data base. The sectorial EDGAR inventories were then grouped into five broad source categories: energy, transportation, industries, residential activities, and other sources (agriculture, waste, and biomass burning). Details of the EDGAR emission sectors and their grouping into the model source categories are included in Table S3 of the Supplementary materials. Fig. S1 shows the emissions of $PM_{2.5}$ from each grouped source. Speciation was performed before the emissions were lumped into the five broad source groups. These gridded annual emissions were remapped to the CMAQ model grids. An in-house preprocessor was used to generate hourly emissions based on monthly (Zhang et al., 2007b), weekly (Wang et al., 2010) and diurnal (Olivier et al., 2003) temporal allocation profiles. This temporal allocation approach has been used in a previous CMAQ modeling study for China (Zhang et al., 2012). It should be noted that the resolution of EDGAR emissions is coarser than the resolution of the finest domain. It does not change the locations and rates of emissions, but allows yield more detailed spatial distribution results by taking advantage of the higher resolution of land use, biogenic emissions and meteorology. This approach has been used by other studies (for example, Li et al., 2013).

The base year of EDGAR emission is 2008. The number of vehicles increased rapidly from ~1.5 million to ~4.1 million (Zhang, 2013) between 2008 and 2012 with further increases likely in later years. This rapid increase by a factor of 2.7 in the number of vehicles warrants an adjustment of the vehicle emissions as they are much higher than uncertainties in reported vehicle emission inventories (Zhao et al., 2011b). Thus, the emission from the transportation source category at each grid cell is adjusted uniformly by a factor of 2.7. As higher emission vehicles are phased out and newer (cleaner) vehicles are adopted in China (the Chinese national emissions standards enacted in 2010 are equivalent to EURO 4), this approach may slightly over-estimate emissions from on-road vehicles. More accurately estimating the change in the vehicle emissions through emissions testing and roadside monitoring is beyond the scope of the current study. Emissions from other source sectors were not adjusted in the EDGAR emissions inventory. While this static treatment could be a potential source of error in model results, projected emission inventories might not represent actual emissions in 2013 better than the 2008 inventory due to large uncertainties in the emission activities and the emission factors used in these calculations.

MEGAN v2.04 (Guenther et al., 2006) was used to generate biogenic emissions driven by WRF meteorology predictions. Windblown dust emissions from soil erosion were generated using an in-house emission processor as described in Zhang et al. (Zhang et al., 2012). WRF initialization data were used to provide the 16-category soil type distribution and 20-category land use/land cover data. Soil moisture and surface frication velocity from WRF simulation were used to adjust windblown dust emission.

The initial conditions for air quality simulations for all the three nested domains and the boundary conditions were generated with default CMAQ profiles that represent relatively clean tropospheric concentrations. Boundary conditions for the 12-km and 4-km domains were generated using CMAQ results from their respective parent domains.

2.4. Simulations conducted

Firstly, a simulation without any modification to CMAQ model is conducted to run as a base case, which is used for model validation against observations. Then, the source-oriented CMAQ model for primary particles is applied to determine the fractional contributions of individual EDGAR source sectors to EC, primary OC (POC), and total primary $PM_{2.5}$ mass. The primary source apportionment code is applied in all three nested domains. Although the results presented in Section 3 shows contributions to 5 lumped emission source groups, the primary source apportionment simulation tracks all EDGAR source sectors separately to calculate the contributions from the lumped sources during the post-processing step. Lastly, source apportionment results to secondary nitrate and sulfate are obtained from the combination of non-source-oriented simulation for the 36 km resolution domain and source-oriented simulations for 12 km and 4 km domains. Boundary conditions of NO_x, SO_2, nitrate and sulfate entering the 12 km domain, as determined by the 36 km simulation, are tracked separately as "upwind sources" to differentiate them from the local source categories within the 12-km domain. The reported upwind contributions in the following discussion are actually contributions from sources outside the 12-km domain.

3. Results and discussion

3.1. Model performance

Observed meteorological data were downloaded from the National Climatic Data Center (NCDC) (ftp://ftp.ncdc.noaa.gov/pub/data/noaa/). 8 stations with observations every three hours were available for the 4 km domain as shown in inlet (a) of Fig. S1. Only one station was available near the city center of Xi'an. Table 1 shows the performance statistics of wind speed (WSPD) and wind direction (WDIR) at 10 m above surface based on the 4 km domain results and all available observations. The statistics include mean observation (OBS), mean prediction (PRE), mean bias (MB), gross error (GE), and root mean square error (RMSE). Wind speeds were as low as 2.83 m s^{-1} during the episode. The model slightly overpredicts wind speed with a MB of 0.19 m s^{-1}. Performance on wind speed meets the benchmarks suggested by Emery et al. (2001) while the bias for wind direction is slightly larger than the target benchmarks. Overall, the model performance is similar to other studies using WRF (Fast et al., 2006; Misenis and Zhang, 2010; Zhang et al., 2014a).

Observed concentrations of SO_2, NO_2, $PM_{2.5}$ and PM_{10} concentrations were downloaded from the Xi'an Environmental Monitoring Center (http://www.xianemc.gov.cn/) to validate the model simulation. Locations of the 12 observation sites are shown in Fig. S2. It should be noted that all sites are located in dense population centers to support the goal of broadcasting a relevant air pollution index to the public.

Table 1
Performance statistics of wind speed (WSPD) and wind direction (WDIR) for January 2013. Values in parenthesis are suggested benchmarks by Emery et al. (2001).

Variables	Statistics				
	OBS	PRE	MB	GE	RMSE
WSPD (m s^{-1})	2.83	3.01	0.19 (≤±0.5)	1.38 (≤2.0)	1.85 (≤2.0)
WDIR (deg)	194.19	177.65	−11.12 (≤±10)	49.30 (≤±30)	67.83

OBS: mean observation. PRE: mean prediction. MB: mean bias. GE: gross error. RMSE: root mean square error.

Fig. 2 shows the comparison of observed and predicted 24-h average $PM_{2.5}$ concentrations. The observed $PM_{2.5}$ concentrations in January 2013 are extremely high throughout all sites. The maximum concentrations at Gaoya, Gaoxin, and Jingkai are close to or greater than 500 μg m^{-3}. Concentrations at other sites are lower, with maximum values of ~400 μg m^{-3}. The model generally captures the day-to-day variations of the $PM_{2.5}$ concentrations at all stations but under-predicts the extreme high concentrations. Underestimation of the extreme high concentrations could be due to various reasons, including emission inventory uncertainties, coarse resolution of air quality model (1 km or even 250 m may be needed for localized high concentrations) (Joe et al., 2014), meteorology uncertainties, and exclusion of the interactions between meteorology and aerosols especially for such an extreme event (Zhang et al., 2014b). Relatively small spatial gradients of $PM_{2.5}$ were predicted at all sites, with the concentration changes in the 9 grid cells surrounding each site smaller than 10%. Due to the lack of observations, model performance on $PM_{2.5}$ components is not validated. A comparison with observations during different periods (Cao et al., 2012; Han et al., 2010; Shen et al., 2009, 2011) (see Table S4) shows that the predicted ratios of EC and nitrate to total $PM_{2.5}$ concentrations are within the range of observations. Predicted total OC is lower mostly due to the under-prediction of secondary organic aerosol (SOA) and sulfate is lower as well. Since the episodes are different and emissions in Xi'an changed dramatically, we believe the results are acceptable.

A comparison of predicted and observed concentrations of NO_2, SO_2, and PM_{10} is shown in Figs. S3–S5 of Supplemental material. Generally, the model reproduces the measured trends of these species with under-prediction of NO_2 concentrations. As a secondary product of chemical reactions, NO_2 underestimation is possibly caused by both emissions and the chemical mechanism used. It has been reported that OH stabilizing processes in China are missing and oxidation of the atmosphere is underestimated in current models (Hofzumahaus et al., 2009). Table 2 summarizes the model statistical performance for gas and PM species at the 12 observation sites using the metric of mean fractional biases (MFB). MFB values of gas phase species vary greatly among stations for the same species. As the predictions show little spatial gradients near the stations, it is likely that some stations are more influenced by near-by emissions sources whose impact cannot be captured with 4 km grid resolution, or some emissions are missing in the EDGAR inventory. The numbers of stations with under-predicted and over-predicted SO_2 concentrations are comparable. NO_2 is under-predicted except at Jingkai, Changan, and Yanliang. MFB values

Table 2
Mean fractional biases (MFB) of gas and PM species at 12 observation sites in Xi'an within the 4 km domain. MFB = $(2/N)\sum(P_i - O_i)/(P_i + O_i)$.

Stations	NO_2	SO_2	$PM_{2.5}$	PM_{10}
Gaoya	−0.90	−0.65	−0.28	−0.22
Xingqing	−0.61	−0.47	0.12	−0.11
Fangzhi	−0.81	−0.03	0.05	−0.11
Xiaozhai	−0.27	−0.46	0.25	−0.17
Tiyuchang	−0.66	−0.01	0.06	−0.14
Gaoxin	−0.46	0.04	−0.22	−0.35
Jiankai	0.19	0.48	−0.14	0.07
Changan	0.07	−0.04	0.15	0.12
Yanliang	0.48	0.25	−0.33	−0.26
Lintong	−1.27	−0.39	−0.35	−0.04
Qujiang	−0.85	0.45	0.05	−0.08
Guangyun	−0.79	0.15	−0.22	−0.29

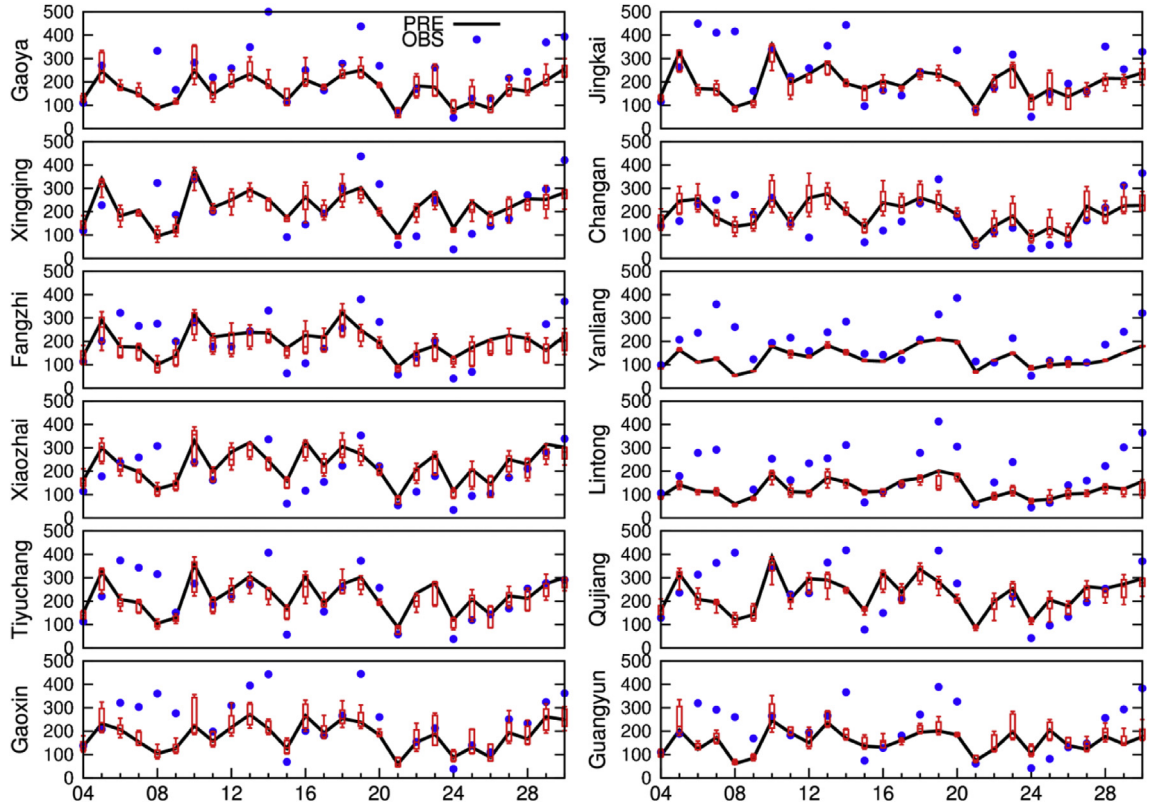

Fig. 2. Predicted and observed 24-h average $PM_{2.5}$ mass concentrations in Xi'an. Horizontal axis shows the day of the month, and vertical axis shows the concentrations of $PM_{2.5}$ mass in units of μg m^{-3}. Solid lines are predicted concentrations at the exact grid cells where the stations are located. The box–whisker plot shows the minimum, maximum, median and inner 50% quartile of the concentrations within 3 grid cell by 3 grid cell regions that surround the observation stations.

for $PM_{2.5}$ and PM_{10} are all within the model guidance and comparable to US values (Boylan and Russell, 2006; Zhang et al., 2014a).

3.2. Regional source contributions to primary $PM_{2.5}$ components

Fig. 3(a) shows the predicted episode-average concentrations of $PM_{2.5}$ total mass and its major components in the 4-km domain surrounding Xi'an. Monthly averaged wind field is also shown in the panel. The Guanzhong plain is separated from north and south sides with very low wind speeds at the connection areas, while pollutants could be transported from the east entrance of the plain by high wind speeds. Monthly $PM_{2.5}$ concentrations were up to >200 μg m^{-3} during this severely polluted episode. High $PM_{2.5}$ concentrations occurred in the urban Xi'an area, the industrial area between Xi'an and Tongchuan to the north of Xi'an, and along the transportation corridor from Xi'an to Baoji to the west. Concentrations in the north area and south area of Shaanxi province covered by the 4-km domain were around 40 and 100 μg m^{-3}, respectively. Major industrial activities between Xi'an and Tongchuan are coal mining, cement production, power generation, and non-ferrous metal smelting with intensive emissions of primary PM and precursors for secondary inorganic PM. The highway and railroad across Shaanxi province from west to east is the busiest transportation corridor connecting West China and East China (See Fig. S2).

Predicted elemental carbon (EC) concentrations are 4–5 μg m^{-3} within the entire Guanzhong plain with the highest concentrations in the urban Xi'an area as shown in Fig. 3(b). Fig. 3(c) shows the concentrations of primary organic carbon (POC) which have a similar spatial pattern as EC but with a maximum concentration of ~20 μg m^{-3}. A factor of 1.4/1 was used for the conversion of POA to POC (Turpin and Lim, 2001). Total organic aerosol (OA) has the same pattern as POC with concentrations of 25–35 μg m^{-3} in Xi'an as shown in Fig. 3(d). SOA predicted during January 2013 is small (with a maximum of less than 2 μg m^{-3}) compared to total OA. SOA concentrations during extreme events in other places of China have been reported (Sun et al., 2014), but it is not clear in Xi'an during to lack of observations. More studies are needed on SOA modeling in China, but the topic is not covered in this study. Episode average sulfate concentrations shown in Fig. 3(e) include both primary and secondary sulfate. The highest predicted concentrations of sulfate are in the urban Xi'an area and the industrial area between Xi'an and Tongchuan. The highest concentrations of ~18 μg m^{-3} are due to contributions from significant primary emissions on top of a regional secondary sulfate background. Section 3.3 discusses the sulfate sources in more details. Nitrate and ammonium concentrations are uniformly distributed in the Guanzhong Plain between the Losses Plateau to the north and the Qingling Mountains to the south, with maximum concentrations of 22 and 12 μg m^{-3}, respectively. Fig. 3(h) shows the concentrations of other $PM_{2.5}$ components other than the explicit species ($PM_{2.5}$ Other), which are 60–140 μg m^{-3} in Xi'an area and 30–50 μg m^{-3} in the Guanzhong Plain.

Fig. 4 shows the predicted source contributions to $PM_{2.5}$ EC. EC emitted from the energy sector contributes less than 0.1 μg m^{-3} in urban Xi'an as shown in Fig. 4(a). Industrial sources contribute as much as 1.8 μg m^{-3} of EC near urban Xi'an and the industrial area to the north, as shown in Fig. 4(b). Contribution of transportation is more regional in a belt shape from east to west along the Guanzhong Plain with the highest concentration of 0.45 μg m^{-3} near urban Xi'an where traffic density is the highest. Residential activities, such as burning coal and wood for cooking and heating, are the major contributor to EC with a maximum concentration of 4.5 μg m^{-3} as shown in Fig. 4(d). Fig. 4(e) indicates that windblown dust also contributes ~0.2 μg m^{-3} to EC in Xi'an area. Fig. 4(f) shows that other sources including agriculture, biomass fires, and waste burning are not significant sources of EC in the episode.

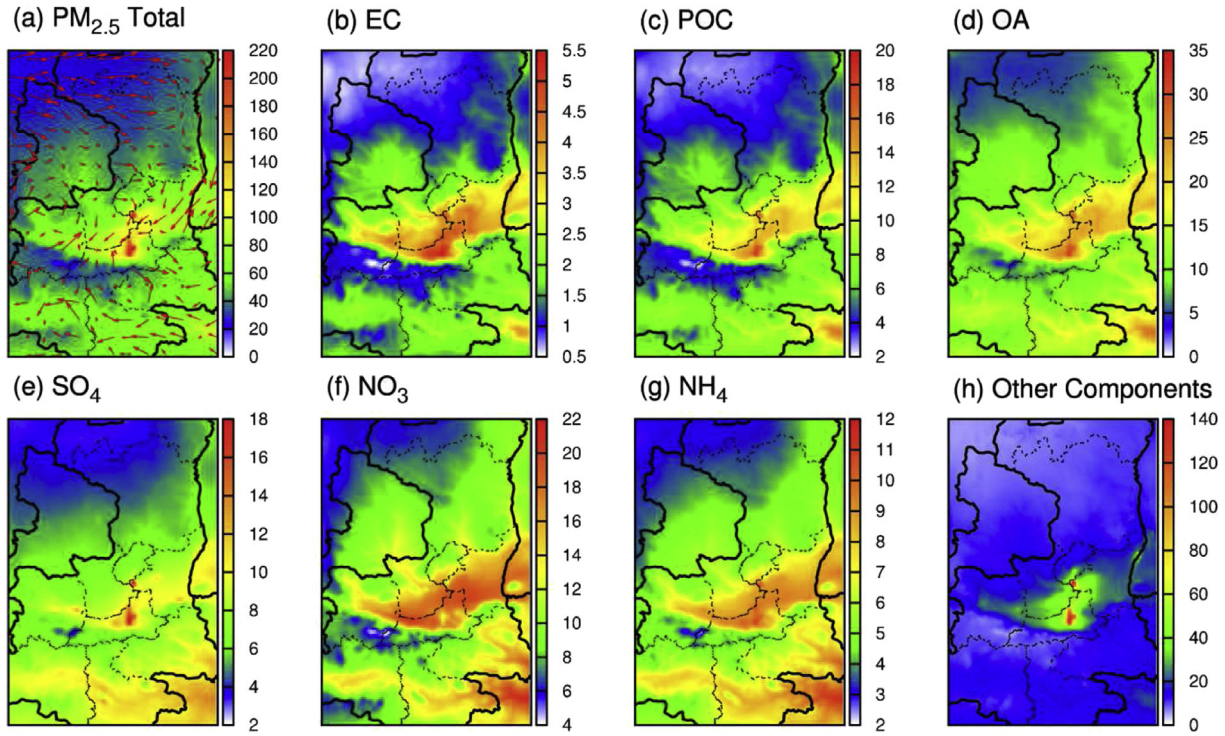

Fig. 3. Episode averaged concentrations of $PM_{2.5}$ mass and its major components. (a) also shows the monthly averaged surface wind field. Units are μg m^{-3}. The scales of the panels are different.

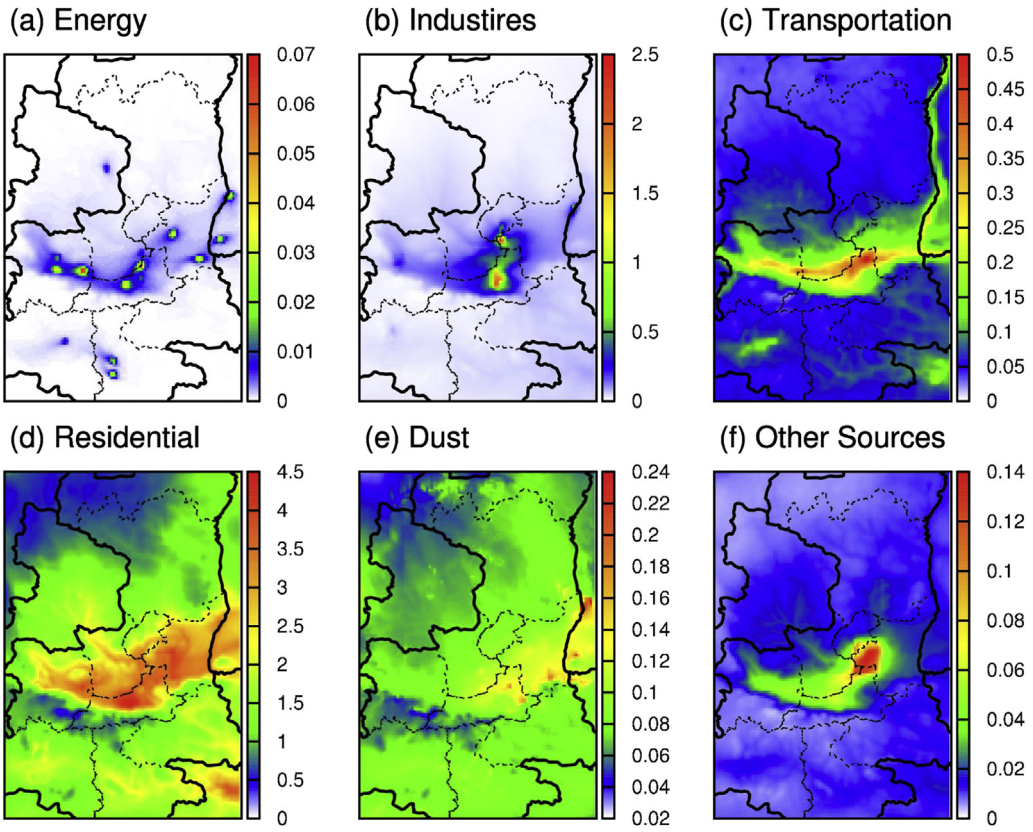

Fig. 4. Episode averaged contributions to $PM_{2.5}$ EC. Units are μg m^{-3}. The scales of the panels are different. (Note: Residential category (d) contains contributions from residential wood combustion. (f) "Other Sources" indicates contribution from inexplicit sources including agriculture, biomass fires, and waste burning as well as upwind sources. The same for Fig. 5 and 6.).

Fig. 5 shows the source types contributing to POC in January 2013. The general spatial pattern of POC contributions from each source is similar to that of EC. Industries (Fig. 5(b)) and residential activities (Fig. 5(d)) are the major sources, contributing to ~4 and 12 μg m^{-3}, respectively. Contributions from transportation (Fig. 5(c)), dust (Fig. 5(e)), and other sources (Fig. 5(f)), are ~0.5 μg m^{-3}, while contributions from energy production (Fig. 5(a)) are very small. Generally, patterns of contributions from various source types to other primary components are similar to those of EC and POC since they are tracked together in the model with different profiles. As shown in Fig. 6, the highest contributions to primary $PM_{2.5}$ "other components" such as crustal material are associated with industrial activities (~100 μg m^{-3}), residential activities (~10 μg m^{-3}), windblown dust (12 μg m^{-3}), and "Other" sources (~7 μg m^{-3}).

3.3. *Regional source contributions to $PM_{2.5}$ nitrate and sulfate*

Nitrate and sulfate are secondary PM components that account for a significant fraction of $PM_{2.5}$ total mass. Fig. 7 shows the episode averaged regional contribution that each source category makes to $PM_{2.5}$ nitrate in the 4-km domain. The energy sector is the dominant nitrate source, accounting for ~10 μg m^{-3}. High nitrate concentrations from energy production are evenly distributed in the Guanzhong Plain and much lower concentrations are distributed in the valley areas to the south and north. Industrial activities make the second largest contribution to nitrate with concentrations of ~3.5 μg m^{-3} over urban Xi'an area as shown in Fig. 7(b). Transportation and residential activities each contribute >2 μg m^{-3} to total nitrate. Contributions from other sources including agriculture, biomass, and waste burning are relatively small as shown in panel (e) of Fig. 7. Fig. 7(f) shows the contributions from primary nitrate and nitrate from upwind sources. Primary nitrate concentrations are very small compared to upwind sources. The spatial distribution of nitrate in Fig. 7(f) suggests that nitrate from upwind sources entering the Guanzhong plain from the east is a significant source of nitrate in Xi'an.

Fig. 8 shows the contributions of different source types to monthly averaged $PM_{2.5}$ sulfate in the 4 km domain over Xi'an. Panels 8 (a–d) show the concentration of sulfate formed by secondary reactions from SO_2 emissions from the indicated source category. Energy production is the dominant source with a contribution of up to 5 μg m^{-3} throughout the Guanzhong plain and the southeast boundary of the 4 km domain. The concentrations in Northern Shaanxi are ~2 μg m^{-3} over the Losses Plateau. Spatial distributions of sulfate from industry, transportation, and residential activities are similar with maximum values of 2, 0.09, and 1 μg m^{-3}, respectively. Panel 8 (f) shows the contributions of primary sulfate sources and sulfate sources upwind of the 12 km domain to concentrations in the Xi'an region. Primary sulfate concentrations are isolated in the vicinity of the emissions source but reach peak concentrations of 9–10 μg m^{-3} above the upwind signal. Sulfate transported from upwind sources has a much smoother regional distribution than primary sulfate indicating that it formed through the oxidation of SO_2 from upwind sources. The concentration of the upwind sulfate is 4–5 μg m^{-3} over the 4 km domain. Resolving the primary sulfate contributions from upwind sources and the contribution of each upwind source type or region requires further investigation for the design of control strategies.

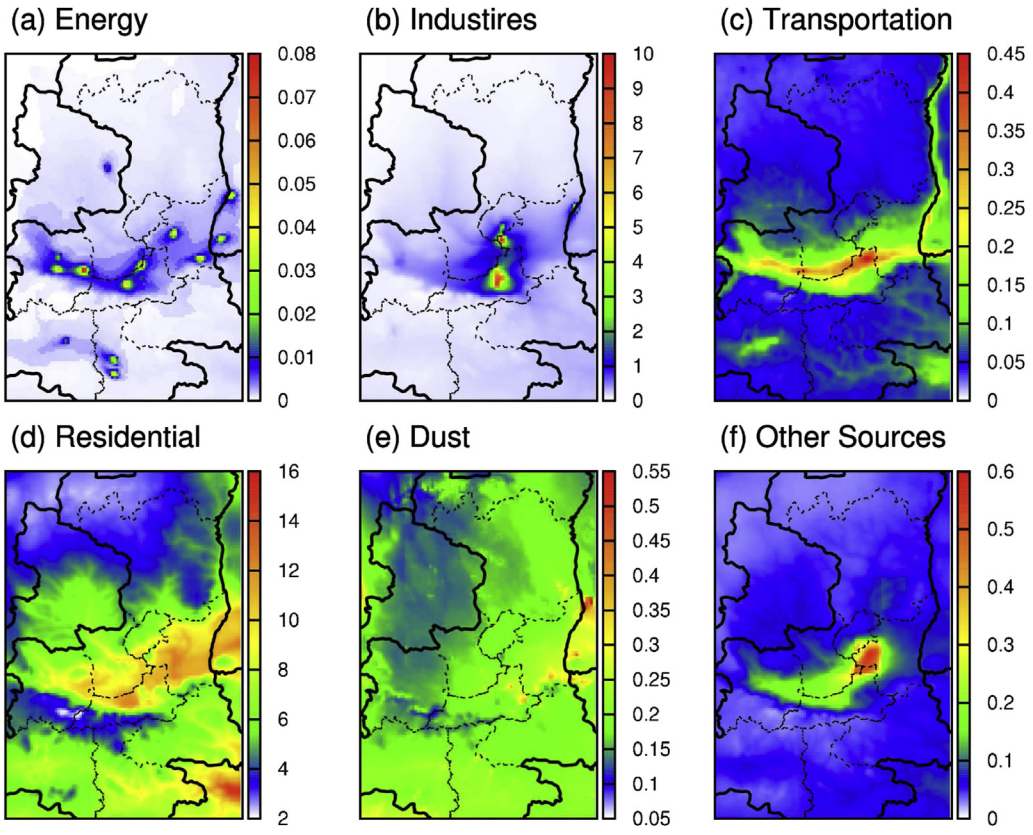

Fig. 5. Episode averaged contributions to $PM_{2.5}$ OC. Units are μg m^{-3}. The scales of the panels are different.

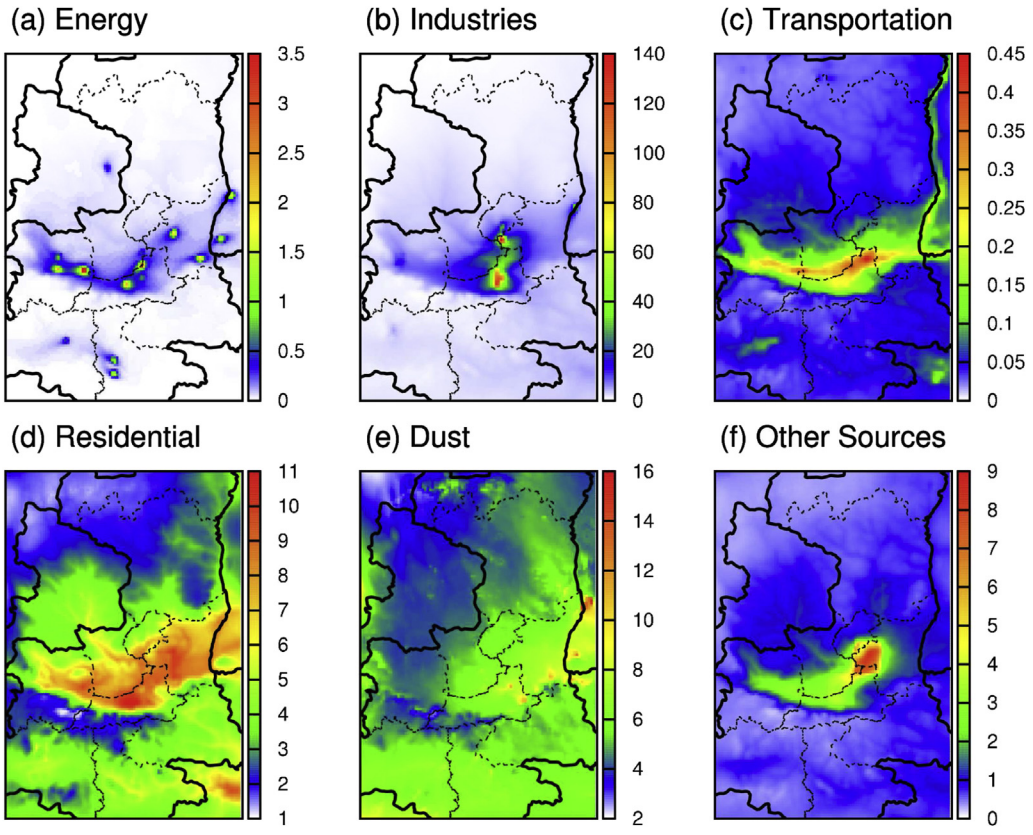

Fig. 6. Episode averaged contributions to primary $PM_{2.5}$ Other Components. Units are μg m^{-3}. The scales of the panels are different.

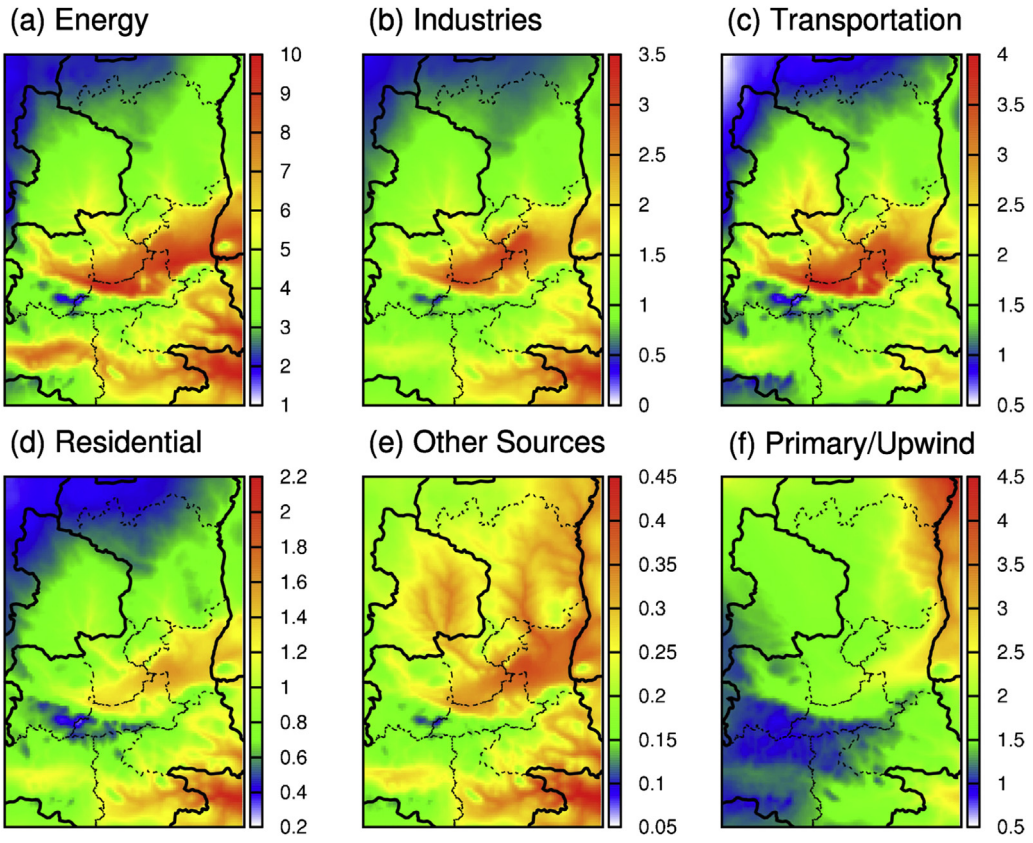

Fig. 7. Episode averaged contributions to $PM_{2.5}$ nitrate. (f) Represents contribution from upwind sources and primary nitrate. Units are μg m^{-3}. The scales of the panels are different. (Note: Residential category (d) contains contributions from residential wood combustion. (e) "Other sources" indicates contribution from inexplicit sources including agriculture, biomass fires, and waste burning. The same for Fig. 8.).

As discussed above, energy production is the dominant source for both $PM_{2.5}$ nitrate and sulfate concentrations, followed by industry and residential activities. Transportation contributes to a significant portion of nitrate concentrations but has very little contribution to sulfate concentrations based on this study. In additional to the local sources, long range transport is also important in the Guanzhong plain as reported in Ying et al. (2014). Due to the unbalanced population and development between the East coastal areas and the Northwest, the energy consumption, industry and transportation are much more intensive in East China. Further analysis of model results from the parent domains indicates that the upwind source contributions to nitrate and sulfate are mostly from East China.

3.4. Regional source contributions to $PM_{2.5}$ total mass

To better provide information for policy makers, the contribution of each source to $PM_{2.5}$ total mass is shown in Fig. 9. It should be noted that this study only conducts source apportionment to primary components and secondary nitrate and sulfate, thus the contributions to $PM_{2.5}$ total mass are based on sources of these species only. Sources to secondary ammonium and SOA are not resolved and they are grouped to "Other" together with inexplicit sources and upwind contributions. Energy contributes to ~16 μg m^{-3} in the Guanzhong plain (8%) as shown in Fig. 9(a). Industries contribute to 60% in industrial region. Contribution from transportation is up to 5.5 μg m^{-3} evenly in the valley. Residential activities are the secondary largest source, accounting for 30–40 μg m^{-3}. Contributions from windblown dust are 10–12 μg m^{-3} (see Fig. 9(e)). As illustrated in Fig. 9(f), unresolved $PM_{2.5}$ components are ~30 μg m^{-3}, which account for ~15% to the total $PM_{2.5}$ mass. More studies should be done in future to fully decompose the unresolved part.

3.5. Source contributions at city center of Xi'an

The Xi'an urban area is the region of greatest interest in the current study since it has the highest population density in the model region. Fig. 10 shows the predicted time series of relative contributions to major $PM_{2.5}$ components in urban Xi'an. The results are daily averaged concentrations at the grid cell containing the urban center (as shown in the inset of Fig. 1).

Maximum daily-averaged EC concentrations can reach as high as 8 μg m^{-3} in central Xi'an. Industry contributed 20–30% of the EC concentrations while transportation accounted for ~5%. Residential activities including winter heating and cooking using wood, coal and natural gas were the most import sources of EC, accounting for 60–70% throughout the monthly simulation. Dust in the "Other Sources" category contributes most of the remaining EC with a maximum contribution of 15% during peak periods. Fig. 10(b) shows that POC concentrations range between 10 and 40 μg m^{-3} in central Xi'an with several cycles of accumulation and partial dilution that mirror the trends in the EC time series. Industry and residential activities are the major POC sources, accounting for 40–50% and 50–60%, respectively throughout the episode. Primary $PM_{2.5}$ mass other than EC and POC (labeled as "Primary $PM_{2.5}$ Other") are ~50–180 μg m^{-3} in January 2013, as show in Fig. 10(c). Industry is the dominating source of this material, with contributions ranging from 60 to 80% on most days. Primary sulfate is an important component from industrial sources, accounting for

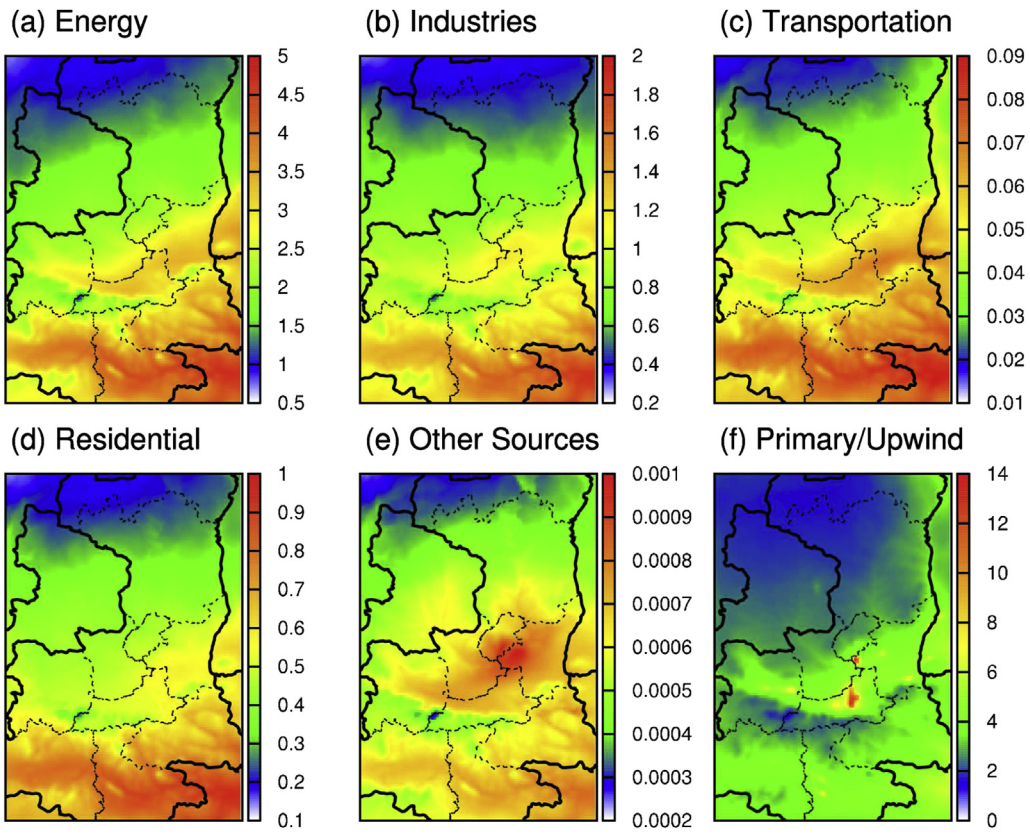

Fig. 8. Episode averaged contributions to $PM_{2.5}$ sulfate. (f) Represents contribution from upwind sources and primary sulfate. Units are $\mu g\ m^{-3}$. The scales of the panels are different.

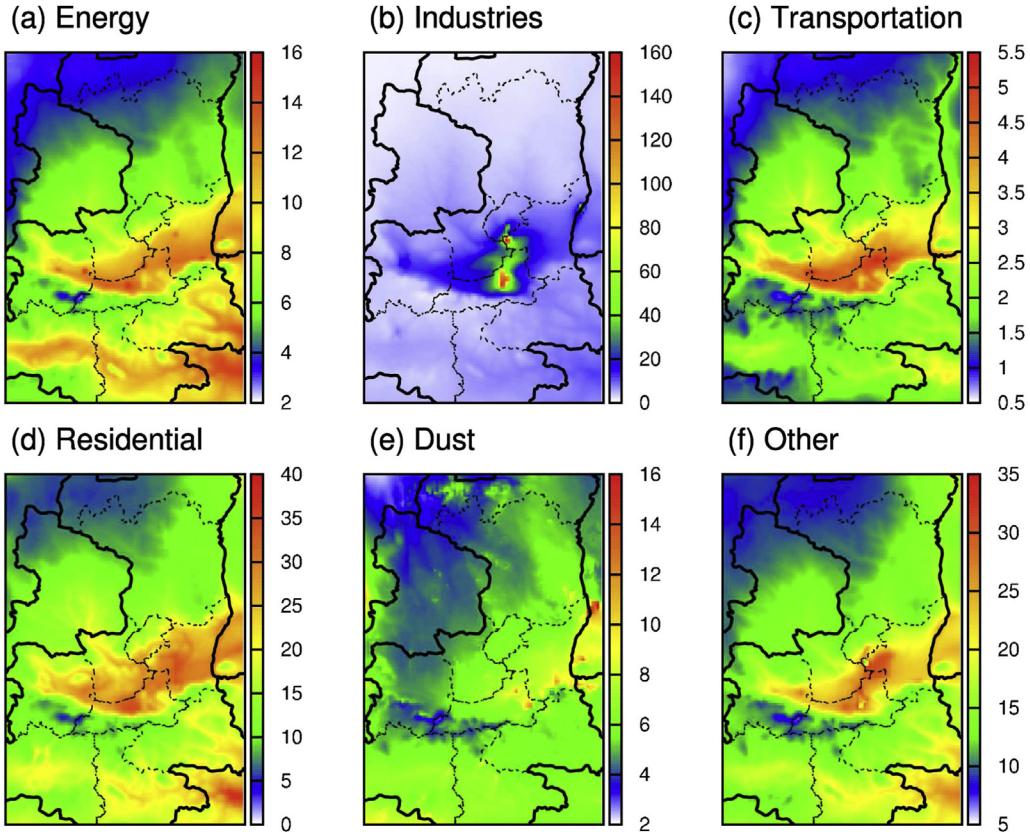

Fig. 9. Episode averaged contributions to $PM_{2.5}$ total mass. (f) Other represents inexplicit sources, unresolved species and upwind contributions. Units are $\mu g\ m^{-3}$. The scales of the panels are different.

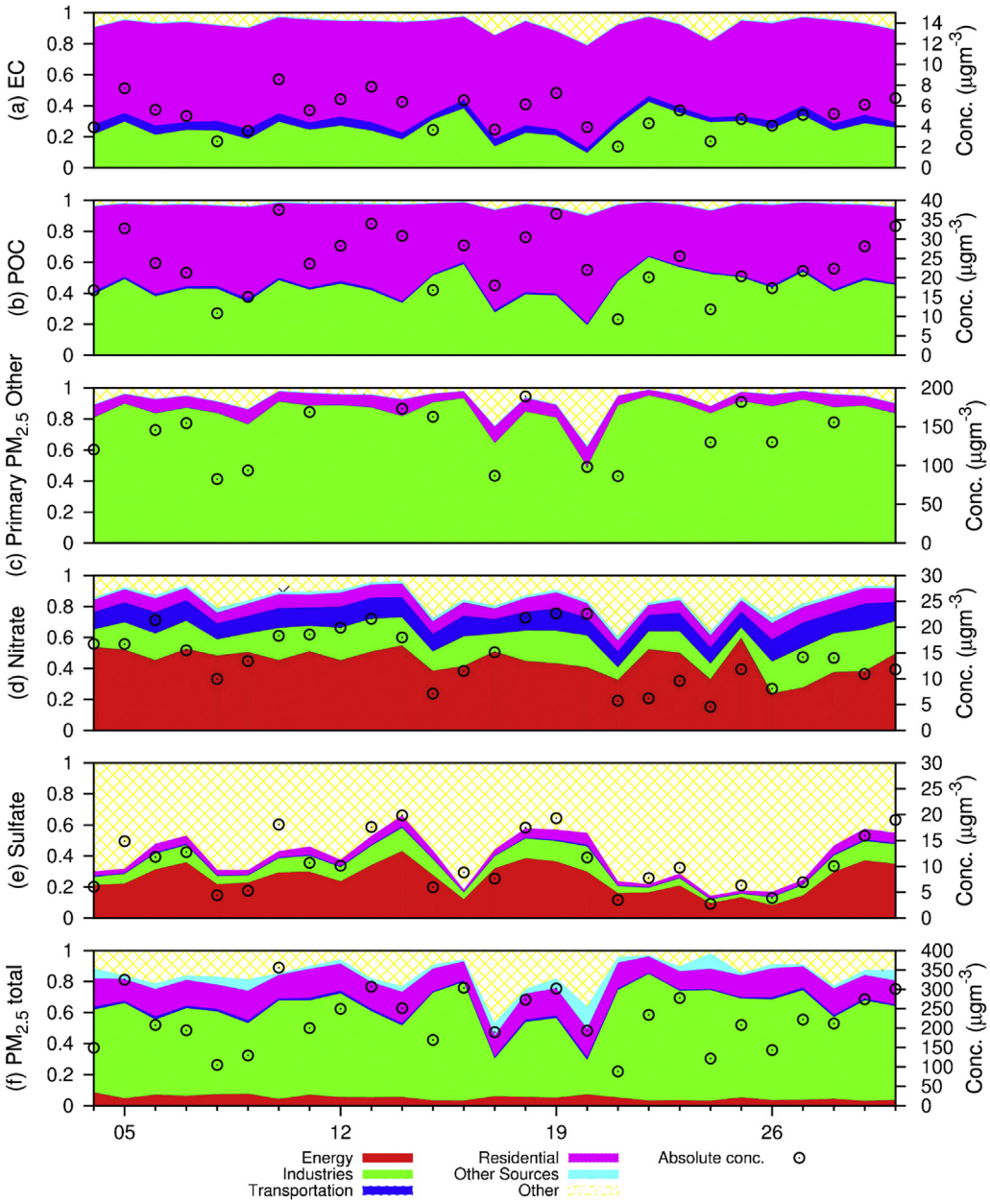

Fig. 10. Time series of relative source contributions to EC, primary OC (POC), total primary $PM_{2.5}$ mass, nitrate and sulfate at city center of Xi'an in January 2013. The black circles are predicted absolute concentrations of these species. Type "Other sources" indicates contribution from inexplicit sources including agriculture, biomass fires, and waste burning. Type "Other" for EC (a), POC (b), and primary $PM_{2.5}$ Other (c) represents contributions from dust and upwind while it represents upwind and primary concentrations for nitrate (d) and sulfate (e). For (f) $PM_{2.5}$ total, "Other Sources" represents dust and inexplicit sources while "Other" represents unresolved species and upwind contributions.

~6–10% based on the profiles used. The minimum industrial contribution was ~50% on 20 January and the maximum was ~90% on 15 January and 23 January. Residential activities contribute to about 10–15% of the "Primary $PM_{2.5}$ Other" component with less variability than the industrial signal. Contributions from dust and upwind sources in the "Other" category to the "Primary $PM_{2.5}$ Other" component ranged between 10 and 30%.

Fig. 10(d) shows the predicted contribution that each source type makes to daily-averaged nitrate concentrations. Nitrate concentrations are generally higher in days before 20 January (up to 25 μg m^{-3}) than in days after 20 January (less than 15 μg m^{-3}). Energy generation is the most important source with contributions to nitrate ranging between 40 and 50% on most of the simulated days. Industrial sources make the second largest contribution, accounting for 10–20%. Contributions from transportation and residential activities are similar (5–10% each). Relative contributions from upwind sources in the "Other" group were relative significant (up to 30%) on days with the lowest absolute nitrate concentrations but were not important (5–10%) on days with the highest absolute nitrate concentrations. Predicted concentrations of sulfate in central Xi'an reached values as high as 20 μg m^{-3} as shown in Fig. 10(e). Energy production was the largest source of sulfate, with contributions reaching 20–40%. Industry is the second largest source of secondary sulfate followed by residential activities, with a combined total contribution of 10–20% from these categories. As mentioned above, primary and upwind sources in "other" group accounted for the majority of sulfate (40–80%).

Fig. 10(f) shows the contributions of different sources to $PM_{2.5}$ total mass. Generally, energy production contributes to less than 10%. Industries are the dominating sources with contributions from 30% to 70%. Transportation contributes only ~3% based on this study. Contributions from residential activities are ~20% throughout the months. Dust and inexplicit sources contribute to 5–10% while the unresolved components and upwind contributions contribute to the rest 10–40%.

4. Conclusion

A severe polluted event during the month of January 2013 in province of Shaanxi China was simulated using the WRF/CMAQ modeling system with source-oriented techniques to quantify the major source contributions to primary and secondary $PM_{2.5}$ components. To the authors knowledge, this is the first regional source apportionment study in Northwest China. Comparison with the observed gas species, $PM_{2.5}$ and PM_{10} shows that the modeling system is able to simulate the observed high $PM_{2.5}$ concentrations reaching ~500 μg m^{-3}. The major components of $PM_{2.5}$ include primary species such as EC, OC and other chemically unresolved components, and secondary species such as sulfate and nitrate.

Contributions from each source sector to primary and secondary inorganic $PM_{2.5}$ components are key information for designing efficient pollution control strategies. This study finds that industrial and residential activities are the dominating sources for EC, POC, and total $PM_{2.5}$ mass. Windblown dust is also a significant source to total $PM_{2.5}$ mass in Xi'an. Energy production is the dominant source of $PM_{2.5}$ nitrate, with additional contributions from upwind sources on days with lower absolute concentrations. Primary sulfate emitted from industrial point sources can reach the concentrations of 10 μg m^{-3} over localized regions near those sources. Concentrations of secondary sulfate from upwind sources are 4–5 μg m^{-3} uniformly in the plain area. The upwind source-identity was not resolved in the current study. Secondary sulfate formed by SO_2 emitted from local sources dominated by energy production accounts for the balance of the total sulfate concentration. Summing up the contributions of different sources to total primary components and secondary nitrate and sulfate, the generally importance of sources to $PM_{2.5}$ total mass are ranked industries > residential activities > energy > dust > transportation besides the contributions of other components, inexplicit sources, and upwind sources.

The ability of the WRF/CMAQ model to predict the observed high $PM_{2.5}$ concentrations demonstrates the ability of a state-of-the-science CTM to act as a useful tool to investigate severe pollution events and provide crucial information needed to design effective control strategies. However, uncertainties associated with model inputs may affect the predicted source contributions. Emissions in Asia based on top-down method have significant uncertainties (Ohara et al., 2007; Zhang et al., 2009; Zhao et al., 2011a). China specific source profiles are generally not available, leaving large fraction of $PM_{2.5}$ mass species categorized as "unknown". Future studies should focus on reducing the uncertainties in the emissions inventory and apply China specific data to improve the model performance and the accuracy of source apportionment information. In addition, measurement-based source apportionment studies should also be considered to provide additional verification of emission inventories and CTM-predicted source apportionment results. .

Acknowledgment

This study is supported by the '948' project from the State Forestry Administration of China (grant #2013-4-56). The authors thank the Texas A&M Supercomputing Facility (http://sc.tamu.edu) and the Texas Advanced Computing Center (http://www.tacc.utexas.edu/) for providing computing resources.

Appendix A. Supplementary materials

Supplementary materials related to this article can be found at http://dx.doi.org/10.1016/j.atmosenv.2014.08.020.

References

An, X., Zhu, T., Wang, Z., Li, C., Wang, Y., 2007. A modeling analysis of a heavy air pollution episode occurred in Beijing. Atmos. Chem. Phys. 7, 3101–3114.
Berglen, T.F., Berntsen, T.K., Isaksen, I.S., Sundet, J.K., 2004. A global model of the coupled sulfur/oxidant chemistry in the troposphere: the sulfur cycle. J. Geophys. Res. 109.
Boylan, J.W., Russell, A.G., 2006. PM and light extinction model performance metrics, goals, and criteria for three-dimensional air quality models. Atmos. Environ. 40, 4946–4959.
Byun, D., Schere, K.L., 2006. Review of the governing equations, computational algorithms, and other components of the models-3 community multiscale air quality (CMAQ) modeling system. Appl. Mech. Rev. 59, 51–77.
Cao, J.-J., Shen, Z.-X., Chow, J.C., Watson, J.G., Lee, S.-C., Tie, X.-X., Ho, K.-F., Wang, G.-H., Han, Y.-M., 2012. Winter and summer PM2.5 chemical compositions in fourteen Chinese cities. J. Air Waste Manag. Assoc. 62, 1214–1226.
Cao, J.-J., Zhu, C.-S., Chow, J.C., Watson, J.G., Han, Y.-M., Wang, G.-h., Shen, Z.-x., An, Z.-S., 2009. Black carbon relationships with emissions and meteorology in Xi'an, China. Atmos. Res. 94, 194–202.
Cao, J.J., Wu, F., Chow, J.C., Lee, S.C., Li, Y., Chen, S.W., An, Z.S., Fung, K.K., Watson, J.G., Zhu, C.S., Liu, S.X., 2005. Characterization and source apportionment of atmospheric organic and elemental carbon during fall and winter of 2003 in Xi'an, China. Atmos. Chem. Phys. 5, 3127–3137.
Carter, W.P.L., 2000. Documentation of the SAPRC-99 Chemical Mechanism for VOC Reactivity Assessment. Report to the California Air Resources Board. Available at: http://cert.ucr.edu/~carter/absts.htm#saprc99 http://www.cert.ucr.edu/~carter/reactdat.htm.
Chen, D., Cheng, S., Liu, L., Chen, T., Guo, X., 2007. An integrated MM5-CMAQ modeling approach for assessing trans-boundary PM10 contribution to the host city of 2008 Olympic summer games – Beijing, China. Atmos. Environ. 41, 1237–1250.
Chen, Y., Ebenstein, A., Greenstone, M., Li, H., 2013. Evidence on the impact of sustained exposure to air pollution on life expectancy from China's Huai River policy. Proc. Natl. Acad. Sci. 110 (32), 12936–12941. http://dx.doi.org/10.1073/pnas.1300018110.
Emery, C., Tai, E., Yarwood, G., 2001. Enhanced meteorological modeling and performance evaluation for two Texas episodes. In: p.b.E., Internatioanl Corp (Ed.), Report to the Texas Natural Resources Conservation Commission (Novato, CA).
Fan, S.J., Fan, Q., Yu, W., Luo, X.Y., Wang, B.M., Song, L.L., Leong, K.L., 2011. Atmospheric boundary layer characteristics over the Pearl River Delta, China, during the summer of 2006: measurement and model results. Atmos. Chem. Phys. 11, 6297–6310.
Fast, J.D., Gustafson, W.I., Easter, R.C., Zaveri, R.A., Barnard, J.C., Chapman, E.G., Grell, G.A., Peckham, S.E., 2006. Evolution of ozone, particulates, and aerosol direct radiative forcing in the vicinity of Houston using a fully coupled meteorology-chemistry-aerosol model. J. Geophys. Res. Atmos. 111.
Feng, Y.R., Wang, A.Y., Xu, X.D., 2007. The influence of tropical cyclone Melor on PM10 concentrations during an aerosol episode over the Pearl River Delta region of China: numerical modeling versus observational analysis. Atmos. Environ. 41, 4349–4365.
Guenther, A., Karl, T., Harley, P., Wiedinmyer, C., Palmer, P.I., Geron, C., 2006. Estimates of global terrestrial isoprene emissions using MEGAN (model of emissions of gases and aerosols from nature). Atmos. Chem. Phys. 6, 3181–3210.
Han, Y., Cao, J., Lee, S., Ho, K., An, Z., 2010. Different characteristics of char and soot in the atmosphere and their ratio as an indicator for source identification in Xi'an, China. Atmos. Chem. Phys. 10, 595–607.
Han, Y.M., Cao, J.J., Chow, J.C., Watson, J.G., An, Z.S., Liu, S.X., 2009. Elemental carbon in urban soils and road dusts in Xi'an, China and its implication for air pollution. Atmos. Environ. 43, 2464–2470.
Hofzumahaus, A., Rohrer, F., Lu, K., Bohn, B., Brauers, T., Chang, C.-C., Fuchs, H., Holland, F., Kita, K., Kondo, Y., Li, X., Lou, S., Shao, M., Zeng, L., Wahner, A., Zhang, Y., 2009. Amplified trace gas removal in the troposphere. Science 324, 1702–1704.
Hu, J., Wang, Y., Ying, Q., Zhang, H., 2014. Spatial and temporal variability of PM2.5 and PM10 over the North China Plain and the Yangtze River Delta, China. Atmos. Environ. 95, 598–609.
Hu, J., Zhang, H., Chen, S.-H., Ying, Q., Wiedinmyer, C., Vandenberghe, F., Kleeman, M., 2014. Identifying PM2.5 and PM0.1 sources for epidemiological studies in California. Environ. Sci. Technol. 48 (9), 4980–4990.
Joe, D.K., Zhang, H., DeNero, S.P., Lee, H.-H., Chen, S.-H., McDonald, B.C., Harley, R.A., Kleeman, M.J., 2014. Implementation of a high-resolution source-oriented WRF/chem model at the port of Oakland. Atmos. Environ. 82, 351–363.
Kleeman, M.J., Cass, G.R., 2001. A 3D Eulerian source-oriented model for an externally mixed aerosol. Environ. Sci. Technol. 35, 4834–4848.

Li, Li, Chen, Chang-Hong, Huang, Cheng, Huang, Hai-Ying, Li, Zuo-Pan, Fu, Joshua S., Jang, Carey J., Streets, David G., 2008. Regional air pollution characteristics simulation of O3 and PM10 over Yangtze River Delta Region. Environ. Sci. 29, 237–245.
Li, L., Chen, C.H., Fu, J.S., Huang, C., Streets, D.G., Huang, H.Y., Zhang, G.F., Wang, Y.J., Jang, C.J., Wang, H.L., Chen, Y.R., Fu, J.M., 2011. Air quality and emissions in the Yangtze River Delta, China. Atmos. Chem. Phys. 11, 1621–1639.
Li, N., Fu, T.-M., Cao, J., Lee, S., Huang, X.-F., He, L.-Y., Ho, K.-F., Fu, J.S., Lam, Y.-F., 2013. Sources of secondary organic aerosols in the Pearl River Delta region in fall: contributions from the aqueous reactive uptake of dicarbonyls. Atmos. Environ. 76, 200–207.
MEP, 2012a. China National Ambient Air Quality Standards. MEP, Beijing, China.
MEP, 2012b. In: Protection, M.o.E. (Ed.), Technical Regulation on Ambient Air Quality Index (On Trial). MEP, Beijing, China.
Misenis, C., Zhang, Y., 2010. An examination of sensitivity of WRF/Chem predictions to physical parameterizations, horizontal grid spacing, and nesting options. Atmos. Res. 97, 315–334.
Napelenok, S.L., Cohan, D.S., Hu, Y.T., Russell, A.G., 2006. Decoupled direct 3D sensitivity analysis for particulate matter (DDM-3D/PM). Atmos. Environ. 40, 6112–6121.
Ohara, T., Akimoto, H., Kurokawa, J., Horii, N., Yamaji, K., Yan, X., Hayasaka, T., 2007. An Asian emission inventory of anthropogenic emission sources for the period 1980–2020. Atmos. Chem. Phys. Discuss. 7, 6843–6902.
Olivier, J., Peters, J., Granier, C., Pétron, G., Müller, J.F., Wallens, S., 2003. Present and Future Surface Emissions of Atmospheric Compounds.
Poschl, U., 2005. Atmospheric aerosols: composition, transformation, climate and health effects. Angew. Chem. Int. Ed. 44, 7520–7540.
Quan, J., Tie, X., Zhang, Q., Liu, Q., Li, X., Gao, Y., Zhao, D., May 2014. Characteristics of heavy aerosol pollution during the 2012–2013 winter in Beijing, China. Atmos. Environ. 88, 83–89. http://dx.doi.org/10.1016/j.atmosenv.2014.01.058.
Shen, Z., Cao, J., Arimoto, R., Han, Z., Zhang, R., Han, Y., Liu, S., Okuda, T., Nakao, S., Tanaka, S., 2009. Ionic composition of TSP and PM2.5 during dust storms and air pollution episodes at Xi'an, China. Atmos. Environ. 43, 2911–2918.
Shen, Z., Cao, J., Liu, S., Zhu, C., Wang, X., Zhang, T., Xu, H., Hu, T., 2011. Chemical composition of PM10 and PM2.5 collected at ground level and 100 meters during a strong winter-time pollution episode in Xi'an, China. J. Air Waste Manag. Assoc. 61, 1150–1159.
Streets, D.G., Fu, J.S., Jang, C.J., Hao, J.M., He, K.B., Tang, X.Y., Zhang, Y.H., Wang, Z.F., Li, Z.P., Zhang, Q., Wang, L.T., Wang, B.Y., Yu, C., 2007. Air quality during the 2008 Beijing Olympic Games. Atmos. Environ. 41, 480–492.
Sun, Y., Jiang, Q., Wang, Z., Fu, P., Li, J., Yang, T., Yin, Y., 2014. Investigation of the sources and evolution processes of severe haze pollution in Beijing in January 2013. J. Geophys. Res. Atmos. 119, 2014JD021641.
Tang, Y.H., Carmichael, G.R., Seinfeld, J.H., Dabdub, D., Weber, R.J., Huebert, B., Clarke, A.D., Guazzotti, S.A., Sodeman, D.A., Prather, K.A., Uno, I., Woo, J.H., Yienger, J.J., Streets, D.G., Quinn, P.K., Johnson, J.E., Song, C.H., Grassian, V.H., Sandu, A., Talbot, R.W., Dibb, J.E., 2004. Three-dimensional simulations of inorganic aerosol distributions in East Asia during spring 2001. J. Geophys. Res. Atmos. 109.
Tie, X., Geng, F., Peng, L., Gao, W., Zhao, C., 2009. Measurement and modeling of O3 variability in Shanghai, China: application of the WRF-Chem model. Atmos. Environ. 43, 4289–4302.
Turpin, B.J., Lim, H., 2001. Species contributions to PM2.5 mass concentrations: revisiting common assumptions for estimating organic mass. Aerosol Sci. Technol. 35, 602–610.
Wang, G.H., Zhou, B.H., Cheng, C.L., Cao, J.J., Meng, J.J., Li, J.J., Tao, J., Zhang, R.J., Fu, P.Q., 2012. Impact of Gobi desert dust on aerosol chemistry of Xi'an, inland China during spring 2009: differences in composition and size distribution between the urban ground surface and the mountain atmosphere. Atmos. Chem. Phys. Discuss. 12, 21355–21397.
Wang, L.T., Wei, Z., Yang, J., Zhang, Y., Zhang, F.F., Su, J., Meng, C.C., Zhang, Q., 2013a. The 2013 severe haze over the southern Hebei, China: model evaluation, source apportionment, and policy implications. Atmos. Chem. Phys. Discuss. 13, 28395–28451.
Wang, S., Wu, D., Wang, X.-M., Fung, J.C.-H., Yu, J.Z., 2013b. Relative contributions of secondary organic aerosol formation from toluene, xylenes, isoprene, and monoterpenes in Hong Kong and Guangzhou in the Pearl River Delta, China: an emission-based box modeling study. J. Geophys. Res. Atmos. 118, 507–519. http://dx.doi.org/10.1029/2012JD017985.
Wang, X., Liang, X.Z., Jiang, W., Tao, Z., Wang, J.X.L., Liu, H., Han, Z., Liu, S., Zhang, Y., Grell, G.A., Peckham, S.E., 2010. WRF-Chem simulation of East Asian air quality: sensitivity to temporal and vertical emissions distributions. Atmos. Environ. 44, 660–669.
Wang, Y., Ying, Q., Hu, J., Zhang, H., 2014. Spatial and temporal variation of six criteria air pollutants in 31 provincial capital cities in China during 2013–2014. Environ. Int. (Revision submitted).
Wei, X., Liu, Q., Lam, K., Wang, T., 2012. Impact of precursor levels and global warming on peak ozone concentration in the Pearl River Delta Region of China. Adv. Atmos. Sci. 29, 635–645.
Wu, Q., Wang, Z., Chen, H., Zhou, W., Wenig, M., 2012. An evaluation of air quality modeling over the Pearl River Delta during November 2006. Meteorol. Atmos. Phys. 116, 113–132.
Xing, J., Zhang, Y., Wang, S.X., Liu, X.H., Cheng, S.H., Zhang, Q., Chen, Y.S., Streets, D.G., Jang, C., Hao, J.M., Wang, W.X., 2011. Modeling study on the air quality impacts from emission reductions and atypical meteorological conditions during the 2008 Beijing Olympics. Atmos. Environ. 45, 1786–1798.
Yamaji, K., Ohara, T., Uno, I., Tanimoto, H., Kurokawa, J., Akimoto, H., 2006. Analysis of the seasonal variation of ozone in the boundary layer in East Asia using the community multi-scale air quality model: what controls surface ozone levels over Japan? Atmos. Environ. 40, 1856–1868.
Ying, Q., Kleeman, M.J., 2006. Source contributions to the regional distribution of secondary particulate matter in California. Atmos. Environ. 40, 736–752.
Ying, Q., Lu, J., Kaduwela, A., Kleeman, M., 2008. Modeling air quality during the California regional PM10/PM2.5 Air Quality Study (CPRAQS) using the UCD/CIT source oriented air quality model – part II. Regional source apportionment of primary airborne particulate matter. Atmos. Environ. 42, 8967–8978.
Ying, Q., Wu, L., Zhang, H., 2014. Local and inter-regional contributions to PM2.5 nitrate and sulfate in China. Atmos. Environ. 94, 582–592.
Zhang, H., Chen, G., Hu, J., Chen, S.-H., Wiedinmyer, C., Kleeman, M., Ying, Q., 2014a. Evaluation of a seven-year air quality simulation using the weather research and forecasting (WRF)/community multiscale air quality (CMAQ) models in the eastern United States. Sci. Total Environ. 473–474, 275–285.
Zhang, H., DeNero, S.P., Joe, D.K., Lee, H.H., Chen, S.H., Michalakes, J., Kleeman, M.J., 2014b. Development of a source oriented version of the WRF/chem model and its application to the California regional PM10/PM2.5 air quality study. Atmos. Chem. Phys. 14, 485–503.
Zhang, H., Li, J., Ying, Q., Guven, B.B., Olaguer, E.P., 2013. Source apportionment of formaldehyde during TexAQS 2006 using a source-oriented chemical transport model. J. Geophys. Res. Atmos. 118, 1525–1535.
Zhang, H., Li, J., Ying, Q., Yu, J.Z., Wu, D., Cheng, Y., He, K., Jiang, J., 2012. Source apportionment of PM2.5 nitrate and sulfate in China using a source-oriented chemical transport model. Atmos. Environ. 62, 228–242.
Zhang, H., Ying, Q., 2010. Source apportionment of airborne particulate matter in Southeast Texas using a source-oriented 3D air quality model. Atmos. Environ. 44, 3547–3557.
Zhang, H., Ying, Q., 2011a. Contributions of local and regional sources of NO_x to ozone concentrations in southeast Texas. Atmos. Environ. 45, 2877–2887.
Zhang, H., Ying, Q., 2011b. Secondary organic aerosol formation and source apportionment in southeast Texas. Atmos. Environ. 45, 3217–3227.
Zhang, Q., Streets, D.G., Carmichael, G.R., He, K.B., Huo, H., Kannari, A., Klimont, Z., Park, I.S., Reddy, S., Fu, J.S., Chen, D., Duan, L., Lei, Y., Wang, L.T., Yao, Z.L., 2009. Asian emissions in 2006 for the NASA INTEX-B mission. Atmos. Chem. Phys. 9, 5131–5153.
Zhang, Q., Streets, D.G., He, K., Klimont, Z., 2007a. Major components of China's anthropogenic primary particulate emissions. Environ. Res. Lett. 2, 045027.
Zhang, Q., Streets, D.G., He, K.B., Wang, Y., Richter, A., Burrows, J.P., Uno, I., Jang, C.J., Chen, D., Yao, Z.L., Lei, Y., 2007b. NO_x emission trends for China, 1995–2004: the view from the ground and the view from space. J. Geophys. Res. 112, D22306.
Zhang, X., 2013. Shaanxi Statistical Yearbook. In: S.P.B.o. (Ed.), Statistics. China Statistics Press, Beijing, China.
Zhang, X.Y., Cao, J.J., Li, L.M., Arimoto, R., Cheng, Y., Huebert, B., Wang, D., 2002. Characterization of atmospheric aerosol over XiAn in the south margin of the Loess Plateau, China. Atmos. Environ. 36, 4189–4199.
Zhao, B., Xu, J., Hao, J., 2011a. Impact of energy structure adjustment on air quality: a case study in Beijing, China. Front. Environ. Sci. Eng. China 5, 378–390.
Zhao, Y., Nielsen, C.P., Lei, Y., McElroy, M.B., Hao, J., 2011b. Quantifying the uncertainties of a bottom-up emission inventory of anthropogenic atmospheric pollutants in China. Atmos. Chem. Phys. 11, 2295–2308.